Experimental characterization of a silicon photonic biosensor consisting of two cascaded ring resonators based on the Vernier-effect and introduction of a curve fitting method for an improved detection limit

Tom Claes, Wim Bogaerts and Peter Bienstman

Photonics Research Group, Department of Information Technology
Ghent University - imec, Sint-Pietersnieuwstraat 41, 9000 Gent, Belgium
tom.claes@intec.ugent.be

Abstract: We studied a refractive index sensor that consists of two cascaded ring resonators and that works analogously to a Vernier-scale. We implemented it in silicon-on-insulator and experimentally determined its sensitivity to be as high as 2169nm/RIU in aqueous environment. We derived formulas describing the sensor's operation, and introduced a fitting procedure that allows to accurately detect changes in the sensor response. We determined the detection limit of this first prototype to be $8.3\,10^{-6}$RIU.

OCIS codes: (130.3120) Integrated optics devices; (130.6010) Sensors; (230.5750) Resonators

References and links

1. X. Fan, I. M. White, S. I. Shopoua, H. Zhu, J. D. Suter, and Y. Sun, "Sensitive optical biosensors for unlabeled targets: A review," Anal. Chim. Acta **620**, 8–26 (2008).
2. A. J. Qavi, A. L. Washburn, J.-Y. Byeon, and R. C. Bailey, "Label-free technologies for quantitative multiparameter biological analysis," Anal. Bioanal. Chem. **394**, 121–135 (2009).
3. I. M. White and X. Fan, "On the performance quantification of resonant refractive index sensors," Opt. Express **16**, 1020–1028 (2008).
4. M. Iqbal, M. A. Gleeson, B. Spaugh, F. Tybor, W. G. Gunn, M. Hochberg, T. Baehr-Jones, R. C. Bailey, and L. C. Gunn, "Label-free biosensor arrays based on silicon ring resonators and high-speed optical scanning instrumentation," IEEE J. Sel. Top. Quantum Electron. **16**, 654–661 (2010).
5. D. X. Xu, A. Densmore, A. Delâge, P. Waldron, R. McKinnon, S. Janz, J. Lapointe, G. Lopinski, T. Mischki, E. Post, P. Cheben, and J. H. Schmid, "Folded cavity soi microring sensors for highsensitivity and real time measurement ofbiomolecular binding," Opt. Express **16**, 15137–15148 (2008).
6. K. De Vos, J. Girones, T. Claes, Y. De Koninck, S. Popelka, E. Schacht, R. Baets, and P. Bienstman, "Multiplexed antibody detection with an array of silicon-on-insulator microring resonators," IEEE Photon. J. **1**, 225–235 (2009).
7. M. Lee and P. M. Fauchet, "Two-dimensional silicon photonic crystal based biosensing platform for protein detection," Opt. Express **15**, 4530–4535 (2007).
8. T. Claes, J. Girones, K. De Vos, E. Schacht, R. Baets, and P. Bienstman, "Label-free biosensing with a slot-waveguide-based ring resonator in silicon on insulator," IEEE Photon. J. **1**, 197–204 (2009).
9. C. F. Carlborg, K. B. Gylfason, A. Kaźmierczak, F. Dortu, M. J. Bañuls Polo, A. Maquieira Catala, G. M. Kresbach, H. Sohlström, T. Moh, L. Vivien, J. Popplewell, G. Ronan, C. A. Barrios, G. Stemme, and W. Van der Wijngaart, "A packaged optical slot-waveguide ring resonator sensor array for multiplex label-free assays in labs-on-chips," Lab Chip **10**, 281–90 (2010).

10. A. Densmore, M. Vachon, D.-X. Xu, S. Janz, R. Ma, Y.-H. Li, G. Lopinski, A. Delâge, J. Lapointe, C. C. Luebbert, Q. Y. Liu, P. Cheben, and J. H. Schmid, "Silicon photonic wire biosensor array for multiplexed real-time and label-free molecular detection," Opt. Lett. **34**, 3598–3600 (2009).
11. F. Blanco, M. Agirregabiria, J. Berganzo, K. Mayora, J. Elizalde, A. Calle, C. Dominguez, and L. Lechuga, "Microfluidic-optical integrated cmos compatible devices for label-free biochemical sensing," J. Micromech. Microeng. **16**, 1006–1016 (2006).
12. D. Dai, "Highly sensitive digital optical sensor based on cascaded high-q ring-resonators," Opt. Express **17**, 23817–23822 (2009).
13. B. Liu, A. Shakouri, and J. Bowers, "Wide tunable double ring resonator coupled lasers," IEEE Photon. Technol. Lett. **14**, 600–602 (2002).
14. P. Rabiei and W. Steier, "Tunable polymer double micro-ring filters," IEEE Photon. Technol. Lett. **15**, 1255–1257 (2003).
15. P. Dumon, W. Bogaerts, D. Van Thourhout, D. Taillaert, R. Baets, J. Wouters, S. Beckx, and P. Jaenen, "Compact wavelength router based on a silicon-on-insulator arrayed waveguide grating pigtailed to a fiber array," Opt. Express **14**, 664–669 (2006).
16. J. Brouckaert, W. Bogaerts, S. Selvaraja, P. Dumon, R. Baets, and D. Van Thourhout, "Planar concave grating demultiplexer with high reflective bragg reflector facets," IEEE Photon. Technol. Lett. **20**, 309–311 (2008).
17. S. K. Selvaraja, P. Jaenen, W. Bogaerts, D. V. Thourhout, P. Dumon, and R. Baets, "Fabrication of photonic wire and crystal circuits in silicon-on-insulator using 193-nm optical lithography," IEEE J. Lightwave Technol. **27**, 4076–4083 (2009).
18. S. Bhattacharya, A. Datta, J. Berg, and S. Gangopadhyay, "Studies on surface wettability of poly(dimethyl) siloxane (pdms) and glass under oxygen-plasma treatment and correlation with bond strength," IEEE J. Microelectromech. Syst. **14**, 590–597 (2005).
19. W. Bogaerts, D. Taillaert, B. Luyssaert, P. Dumon, J. V. Campenhout, P. Bienstman, D. V. Thourhout, R. Baets, V. Wiaux, and S. Beckx, "Basic structures for photonic integrated circuits in silicon-on-insulator," Opt. Express **12**, 1583–1591 (2004).
20. J. Hu, X. Sun, A. Agarwal, and L. C. Kimerling, "Design guidelines for optical resonator biochemical sensors," J. Opt. Soc. Am. B **26**, 1032–1041 (2009).
21. H. Su and X. G. Huang, "Fresnel-reflection-based fiber sensor for on-line measurement of solute concentration in solutions," Sens. Act. B **126**, 579–582 (2007).

1. Introduction

Label-free photonic biosensors can perform sensitive and quantitative multiparameter measurements on biological systems and can therefore contribute to major advances in medical analyses, food quality control, drug development and environmental monitoring. Additionally they offer the prospect of being incorporated in laboratories-on-a-chip that are capable of doing measurements at the point-of-care at an affordable cost [1, 2].

A crucial component in most of these photonic biosensors is a transducer that can transform a refractive index change in its environment to a measurable change in its optical transmission. Silicon-on-insulator is a material system with many assets for such transducers. First, it has a high refractive index contrast permitting very compact sensors of which many can be incorporated on a single chip, enabling multiplexed sensing. Second, silicon-on-insulator photonic chips can be made with CMOS-compatible process steps, allowing for a strong reduction of the chip cost by high volume fabrication. These sensor chips can therefore be disposable, meaning that the chip is only used once, avoiding complex cleaning of the sensor surface after use.

Typically, a spectral shift of the transmission spectrum of the transducer is used to quantify the measured refractive index change, because this method can be extended to the parallel read-out of multiple sensors in a sensor matrix. An important figure of merit is the transducer's limit of detection, which is given by the ratio of the smallest detectable spectral shift and the sensitivity of the sensor [3]. The latter is a measure for how much the spectrum shifts for a given change of the refractive index.

There exist different types of transducers on silicon-on-insulator that use a variety of methods to achieve a low limit of detection. By using resonant sensors with high quality factors that have very narrow resonance peaks, the smallest detectable spectral shift can be minimized [4, 5, 6, 7]. In [4] a ring resonator sensor is presented that is made with mass fabrication compatible

technology and that has a very low detection limit of $7.6\,10^{-7}$RIU. This sensor has a bulk sensitivity of 163nm/RIU, which is not exceptionally high. However they accomplish a smallest detectable wavelength shift as small as 0.22pm with an optimized sensor design and a very noise resistant optical setup and data analysis. Slot waveguides with enhanced light-matter interaction have been applied to improve the sensitivity of ring resonator sensors with a factor two to four [8, 9], but increased optical losses have prevented them so far from achieving better detection limits than normal ring resonator sensors. Integrated interferometers with large interaction lengths have also proved to be promising [10, 11], with detection limits in the order of 10^{-6}RIU. In [12] a sensor is introduced that consists of two cascaded ring resonators, and it is shown theoretically that it can obtain very high sensitivities thanks to the Vernier-principle. It operates as a digital sensor however, which limits its smallest detectable shift and its detection limit. Previously, a similar cascade of ring resonators was applied in the design of integrated lasers [13] and tunable filters [14].

In this article we introduce a transducer with the same working principle as the one introduced in [12], but by using ring resonators with very large roundtrip lengths, we make it work in another regime that allows to reduce the detection limit.

First, we derive formulas that accurately describe the transmission spectrum of the sensor, and we introduce a fitting procedure that allows to reduce the smallest detectable wavelength shift with an order of magnitude compared to the method presented in [12].

Second, we present the first experimental results of this type of sensor. A first non-optimized prototype was implemented in silicon-on-insulator, and it was measured to have a sensitivity as high as 2169nm/RIU and a detection limit of $8.3\ 10^{-6}$RIU. Although the detection limit is currently not improved compared to that of a single ring resonator sensor [4], we think this first experimental result is promising for future optimized designs regarding the different levels of optimization of single ring resonator sensors and this new sensor. Additionally, as also stated in [12], the very large sensitivity of this sensor makes it very well suited for integration with on-chip dispersive elements such as arrayed waveguide gratings [15] or planar concave gratings [16], giving opportunities for cheaper and more portable sensor read-out.

2. Theoretical analysis of the sensor

The Vernier-scale is a method to enhance the accuracy of measurement instruments. It consists of two scales with different periods, of which one slides along the other one. The overlap between lines on the two scales is used to perform the measurement. It is commonly used in calipers and barometers, and it has also been applied in photonic devices [13, 14].

In Fig. 1 it is illustrated how this concept can be applied to a ring resonator sensor. Two ring resonators with different optical roundtrip lengths are cascaded, so that the drop signal of the first ring resonator serves as the input of the second. Each individual ring resonator has a comb-like transmission spectrum with peaks at its resonance wavelengths. The spectral distance between these peaks, the free spectral range, is inversely proportional to the optical roundtrip of the resonator, so that each resonator in the cascade will have a different free spectral range. As the transmission spectrum of the cascade of the two ring resonators is the product of the transmission spectra of the individual resonators, it will only exhibit peaks at wavelengths for which two resonance peaks of the respective ring resonators (partially) overlap, and the height of each of these peaks will be determined by the amount of overlap.

The complete chip is covered with a thick cladding, with only an opening for one of the two resonators. This sensor ring resonator will act as the sliding part of the Vernier-scale, as its evanescent field can interact with the refractive index in the environment of the sensor, where a change will cause a shift of the resonance wavelengths. The other resonator, the filter ring resonator, is shielded from these refractive index changes by the cladding and will act as the

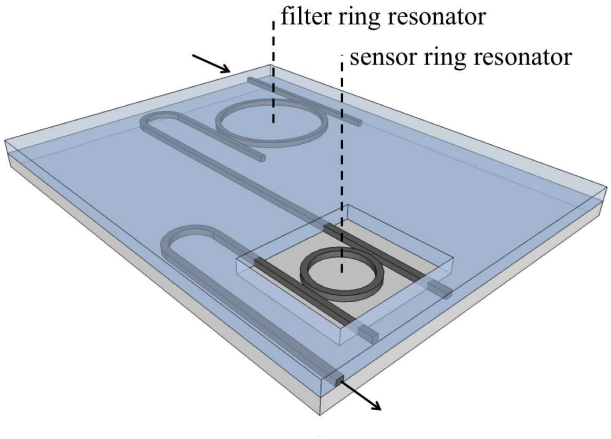

Fig. 1. Illustration of the concept of the photonic sensor consisting of two cascaded ring resonators. Two ring resonators with different optical roundtrip lengths are cascaded. The complete chip is covered with a thick cladding, with only an opening for one of the two resonators. This sensor ring resonator will be exposed to refractive index changes in its environment, while the other resonator, the filter ring resonator, is shielded from these refractive index changes by the cladding.

fixed part of the Vernier-scale. The cascade of both resonators can be designed such that a small shift of the resonance wavelengths of the sensor ring resonator will result in a much larger shift of the transmission spectrum of the cascade.

We can identify two regimes:

The first regime is illustrated on the left side of Fig. 2 and occurs when the free spectral range difference between the two resonators in the cascade is large compared to the full-width at half-maximum of the resonance peaks of the individual resonators. The transmission spectrum of the cascade will then typically exhibit isolated peaks, of which the neighboring peaks are inhibited. The sensor will in this regime behave as a discrete sensor, of which the transmission peak will hop from one filter ring resonance wavelength to another for a changing refractive index. The smallest detectable shift of the transmission spectrum of this sensor is equal to the free spectral range of the filter ring resonator, which forms a limitation to the detection limit of the sensor. The sensor presented in [12] works in this regime.

A second regime occurs however when the free spectral range difference between the two resonators in the cascade is small compared to the full-width at half-maximum of the resonance peaks of the individual resonators. On the right side of Fig. 2 it is illustrated that in this regime a periodic envelope signal is superposed on the constituent transmission peaks. It is proven in appendix A that, if we do not take dispersion into account, the envelope period is given by

$$\frac{fsr_{sensor} \cdot fsr_{filter}}{\left| fsr_{sensor} - fsr_{filter} \right|} \tag{1}$$

where fsr_{sensor} and fsr_{filter} are the free spectral range values of the corresponding individual resonators. Note that in practice the envelope period can not be chosen larger than the available wavelength range of the measurement equipment, so that the second regime typically requires that the cascade consists of resonators with very large roundtrips. In the remainder of this article, we will work with sensors that work in this regime.

In this section we will introduce an analytical formula for the envelope signal, and in section 4 we will show that this formula can be fitted to experimental data, making it possible to

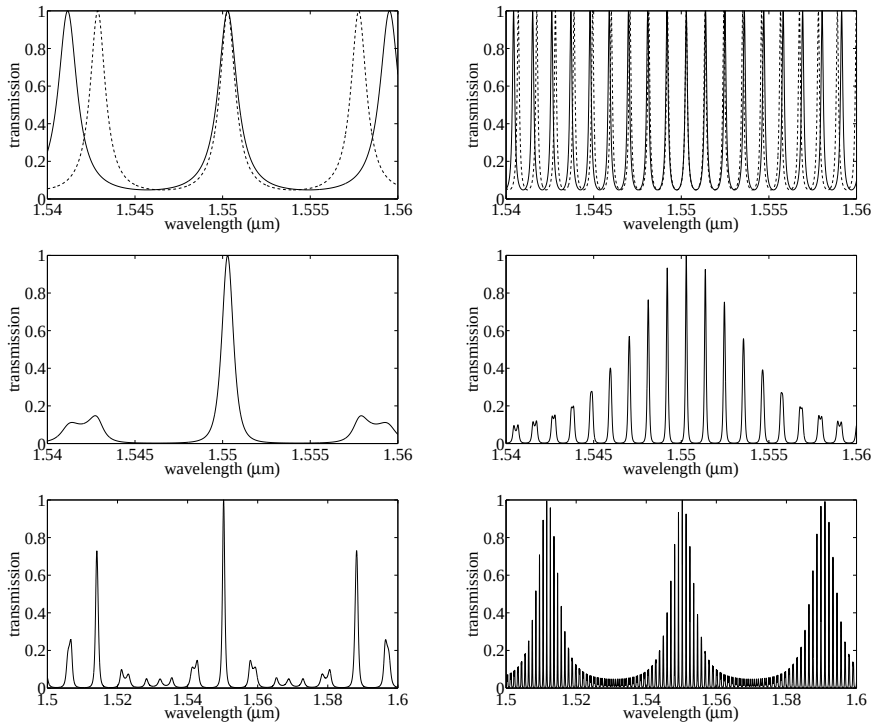

Fig. 2. Calculated transmission spectra that illustrate the operation of the cascade. The graphs on the left side illustrate a first regime that occurs when the free spectral range difference between the two resonators is large compared to the full-width at half-maximum of the resonance peaks of the individual resonators. The graphs on the right side illustrate a second regime that occurs when the free spectral range difference between the two resonators is small compared to the full-width at half-maximum of the resonance peaks of the individual resonators. Top: transmission spectra of the individual filter ring resonator (dashed line) and sensor ring resonator (normal line). Middle: transmission spectra of the cascade of these two resonators in the same wavelength range as the top image, illustrating only one clearly visible transmitted peak in the first regime (left), while in the second regime (right) an envelope signal is superposed on the constituent peaks. Bottom: transmission spectra of the cascade in a larger wavelength range.

continuously track the spectrum of the sensor, allowing a reduction of the detection limit.

As each peak in the transmission spectrum of the individual ring resonators is well approximated by a Lorentzian function, each of the constituent peaks in the transmission spectrum of the cascade can be described as the product of two Lorentzian functions that are shifted compared to each other:

$$T_{constituent}(\lambda) = \frac{t_{max,filter}\frac{fwhm_{filter}^2}{4}}{\frac{fwhm_{filter}^2}{4} + \left(\lambda - \lambda_0 - \frac{\Delta\lambda}{2}\right)^2} \cdot \frac{t_{max,sensor}\frac{fwhm_{sensor}^2}{4}}{\frac{fwhm_{sensor}^2}{4} + \left(\lambda - \lambda_0 + \frac{\Delta\lambda}{2}\right)^2} \tag{2}$$

where t_{max} and $fwhm$ are respectively the transmission at resonance and the full-width at half-maximum of the corresponding individual ring resonator, and where λ_0 and $\Delta\lambda$ are respectively the mean of and the difference between the two resonance wavelengths under consideration from both combs.

If we assume that both ring resonators have the same full-width at half-maximum $fwhm$, it is shown in appendix B that we can identify two different shapes of the constituent peaks, depending on their position in the envelope peak:

If the difference between the resonance wavelengths is larger than the full-width at half-maximum of the individual resonances, $\Delta\lambda > fwhm$, the corresponding constituent peak has two maxima of which the transmission quickly converges to zero for increasing values of $\Delta\lambda$. This situation corresponds to the tails of the envelope, where the transmission is very low.

If however the difference between the resonance wavelengths is smaller or equal than the full-width at half-maximum of the individual resonators, $\Delta\lambda <= fwhm$, Eq. (2) has only one maximum. This situation corresponds to the constituent peaks in the center of the envelope peak, where the transmission is high. In appendix C it is proven that the envelope peak in the transmission of the cascade formed by these maxima is in good approximation given by

$$T_{envelope}(\lambda) = \left(\frac{\sqrt{t_{max,filter} t_{max,sensor}} \left(\frac{FWHM}{2}\right)^2}{\left(\frac{FWHM}{2}\right)^2 + (\lambda - \lambda_{central})^2} \right)^2 \tag{3}$$

with

$$FWHM = 2 \cdot \frac{fwhm \cdot min\left(fsr_{sensor}, fsr_{filter}\right)}{\left| fsr_{filter} - fsr_{sensor} \right|} \tag{4}$$

Here $\lambda_{central}$ is defined as the central wavelength of the envelope peak. Eq. (3) shows that the envelope signal forms a peak described by the square of a Lorentzian function with full-width at half-maximum $FWHM$.

A change of the refractive index in the evanescent field of the sensor ring resonator will cause a shift of the resonance peaks in its transmission spectrum, which will be translated in a much larger shift of the central wavelength of the envelope peak in the transmission spectrum of the cascade. In appendix D it is proven that the sensitivity of the cascaded ring resonator sensor is given by

$$\frac{\partial \lambda_{central}}{\partial n_{env}} = \frac{fsr_{filter}}{fsr_{filter} - fsr_{sensor}} \frac{\frac{\partial n_{eff,sensor}}{\partial n_{env}} \lambda}{n_{g,sensor}} \tag{5}$$

with $\frac{\partial n_{eff,sensor}}{\partial n_{env}}$ the change of the effective index of the sensor ring resonator waveguide due to a change of the refractive index in the environment of the sensor and $n_{g,sensor}$ the group index of the sensor ring resonator waveguide. The sensitivity of the cascaded ring resonator sensor is enhanced with a factor $\frac{fsr_{filter}}{fsr_{filter} - fsr_{sensor}}$ compared to the sensitivity of a single ring resonator sensor. As already stated earlier, in practice the period of the envelope signal of the cascade cannot be chosen larger than the available wavelength range of the measurement equipment. For a given envelope period, Eq. (1) and (5) show that the sensitivity is in good approximation proportional to the optical roundtrip length of the resonators in the cascaded. Note that for an increasing refractive index n_{env} the resonance wavelength of a single ring resonator will always shift to larger wavelengths, while the central wavelength of the envelope peak in the transmission spectrum of the cascade will shift to smaller wavelengths if $fsr_{filter} < fsr_{sensor}$ and to larger wavelengths if $fsr_{filter} > fsr_{sensor}$.

3. Design and fabrication of the device

Our sensor was made in silicon-on-insulator with $2\mu m$ buried oxide and 220nm silicon top layer with CMOS-compatible 193nm optical lithography and dry etching. An elaborate description of the fabrication process can be found in [17]. Fig. 3 pictures the device.

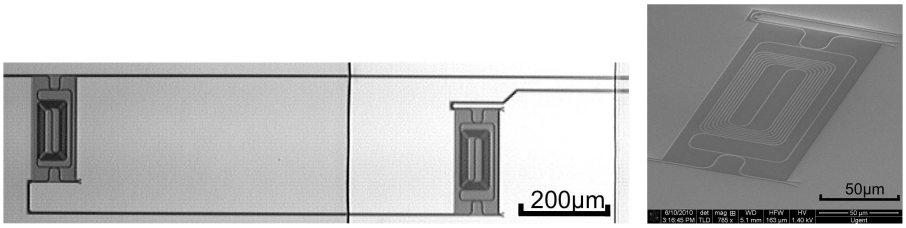

Fig. 3. Left: Optical microscope image of the device fabricated in silicon-on-insulator. Two ring resonators with 2.5mm physical roundtrip length are cascaded, and their footprint is reduced by folding the cavity. The complete chip was covered with 500nm silicon oxide, and an opening was etched to the second ring resonator. Right: Scanning electron microscope image of the second ring resonator with folded cavity.

Two ring resonators are cascaded similar to the concept explained in section 2. In order to work in the second regime mentioned in that section and in order to have an envelope period smaller than the bandwidth of our grating couplers introduced in section 4, the physical roundtrip length of the filter resonator and sensor resonator was respectively chosen to be 2528nm and 2514nm. By folding the cavity [5] their footprint was reduced to only $200\mu m \times 70\mu m$. The resonators consist of 450nm wide single-mode waveguides and each one has two $6\mu m$ long directional couplers with a gap of 180nm between the waveguides. The complete chip was covered with 500nm silicon oxide by plasma deposition and a window was etched to the second resonator in the cascade by consecutive dry and wet etching, so that only the evanescent field of this sensor ring resonator can interact with refractive index changes in the environment of the sensor. Note that this design is suboptimal and only serves as a proof-of-principle. Future work involves optimizing the resonator roundtrips and directional couplers.

4. Experimental characterization

To allow controlled delivery of liquids to the sensor, a microfluidic channel with $600\mu m \times 50\mu m$ cross section was made in PDMS by casting and directly bonded to the sensor chip at $135°C$ after having applied a short oxygen plasma treatment to both surfaces [18]. The liquids were pumped through the channel over the sensor ring resonator with a syringe pump at a $5\mu L/min$ flow rate. The chip was mounted on a temperature-stabilized chuck to avoid drifting of the sensor signal due to temperature variations. A second-order diffractive grating, integrated on the input and output waveguides, is used to couple from a $10\,\mu m$ wide ridge waveguide to a vertically oriented, butt-coupled single-mode fiber. The grating has 10 periods of 630nm with 50nm etch depth. A linear, $150\,\mu m$ long taper is employed as a transition between the ridge waveguide and a 450nm wide photonic wire waveguide. A more detailed description of the grating couplers can be found in [19]. A polarization controller was used to tune the polarization of light from a tunable laser for maximum coupling to the quasi-TE mode of the waveguides, and the optical power transmitted by the sensor was measured with a photodetector.

In Fig. 4 the transmission spectrum of our sensor is plotted. Deionized water was flowing over the sensor. As predicted in section 2, a periodic envelope signal is superposed on the sharp constituent peaks.

The detection limit of a refractive index sensor, the smallest change of the refractive index that can be detected, is often defined as the ratio between the smallest detectable spectral shift of its transmission spectrum and its sensitivity [3]. Next to having a sensor with a large sensitivity, it is thus equally important to be able to measure a small shift of the transmission spectrum. This smallest detectable shift is determined by the shape of the spectrum and the noise, but also

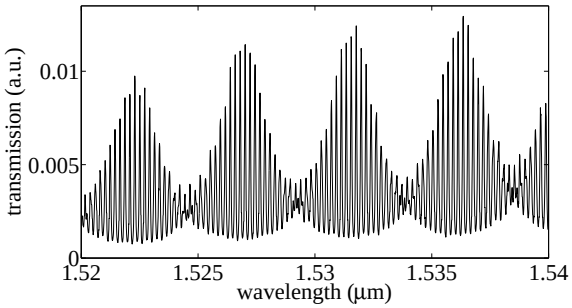

Fig. 4. Measured transmission spectrum of the device as deionized water is flowing over the sensor ring resonator. The height of the envelope peaks varies due to the wavelength-dependent coupling efficiency of the grating couplers.

the method that is adopted to analyze the spectrum has a large impact [20].

Here we will introduce a method to accurately determine the central wavelength of an envelope peak in the transmission spectrum of the cascaded ring resonator sensor, which is based on fitting the formulas derived in section 2 to the measured spectrum. The fitting procedure is illustrated in Fig. 5

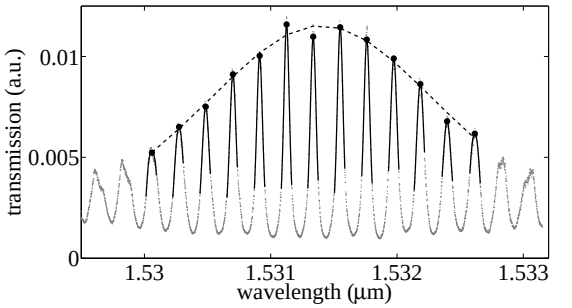

Fig. 5. Illustration of the fitting procedure. In grey a measured transmission spectrum of our device is shown. In a first step Eq. (2) is fitted to the highest constituent peaks, shown by the solid lines. Then the analytical maxima of these fits are determined, shown by the dots. In a second step, Eq. (3) is fitted to the envelope signal formed by these maxima, which is shown by the dashed line. The position of the analytical maximum of that last fit is taken as the central wavelength of the envelope peak.

In a first step, Eq. (2) is fitted to the highest constituent peaks in the transmission spectrum. In Fig. 5 a good correspondence can be observed between the fitted function and the experimental data, which was measured with 1pm wavelength step. By taking the analytical maximum of the fitted function for each of these constituent peaks, the envelope signal is determined in a noise resistant way.

In a second step, Eq. (3) is fitted to the envelope signal that is formed by the output of previous step. In Fig. 5 this fit is shown by the dashed line. The position of the analytical maximum of this function is taken as the central wavelength of the measured envelope peak.

A good measure for the smallest detectable wavelength shift with this method is given by the standard deviation on the fitted central wavelength of the envelope peak. Based on the confidence interval of the fitting parameters returned by our standard fitting software, the smallest

detectable wavelength shift was calculated to be 18pm for the measured spectra of our sensor. Note that this value is an order of magnitude smaller than the distance between the peaks in the spectrum.

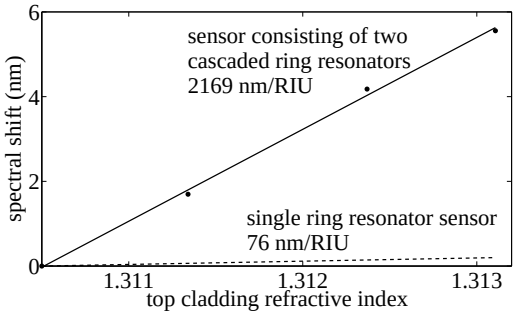

Fig. 6. Shift of the transmission spectrum of the sensor consisting of two cascaded ring resonators as a function of the bulk refractive index in its top cladding. The dots show the shift that was measured by changing the flow between deionized water and aqueous solutions of NaCl with different concentrations, and the solid line represents the linear fit to this experimental data, revealing a sensitivity of 2169nm/RIU. For comparison, the dashed line shows the calculated resonance wavelength shift of a single ring resonator.

To measure the sensitivity of the sensor to changes in the bulk refractive index of its aqueous environment, it was measured how much the envelope peaks in the transmission spectrum shifted when changing between flowing deionized water and three aqueous solutions of NaCl with different concentrations. The refractive index of each of these solutions was calculated [21]. In Fig. 6 the dots indicate the measured shifts as a function of bulk refractive index. A linear function was fitted to the measured shifts, and its slope revealed a sensitivity of 2169nm/RIU. This value corresponds well with the theoretical sensitivity of 2085nm/RIU calculated with Eq. (5). The resonance wavelength shift of a single ring resonator comprised of a 450nm wide waveguide is calculated to be 76nm/RIU, showing the large sensitivity improvement with the presented sensor. The calculation of both mentioned sensitivities is described in appendix E.

The resulting detection limit of our sensor is equal to the ratio of the smallest detectable wavelength shift and the sensitivity, that is 18pm / 2169nm/RIU = 8.3 10^{-6}RIU. Although the detection limit is currently not improved compared to that of a single ring resonator sensor [4], we think this first experimental result is promising for future optimized designs regarding the different levels of optimization of single ring resonator sensors and this new sensor. Additionally, as also stated in [12], the very large sensitivity of this sensor makes it very well suited for integration with on-chip dispersive elements such as arrayed waveguide gratings [15] or planar concave gratings [16], giving opportunities for cheaper and more portable sensor read-out.

5. Conclusions

We studied a refractive index sensor that consists of two cascaded ring resonators and that works analogously to a Vernier-scale. We implemented it in silicon-on-insulator and experimentally determined its sensitivity to be as high as 2169nm/RIU in aqueous environment. We derived formulas describing the sensor's operation, and introduced a fitting procedure that allows to accurately detect changes in the sensor response. We determined the detection limit of this first prototype to be 8.3 10^{-6}RIU.

Appendices

A. Derivation of the analytical function for the period of the envelope signal

When the free spectral range difference between the two resonators in the cascade is small compared to the full-width at half-maximum of the resonance peaks of the individual resonators, a periodic envelope signal is superposed on the constituent transmission peaks in the transmission spectrum of the cascade. To derive the envelope period, we will start from the case displayed in Fig. 7, where the transmission spectra of the two individual ring resonators are plotted. The resonance wavelengths of the resonator with the shortest optical roundtrip (solid line) are denoted λ_{short}, and the resonance wavelengths of the resonator with the longest optical roundtrip (dashed line) as λ_{long}.

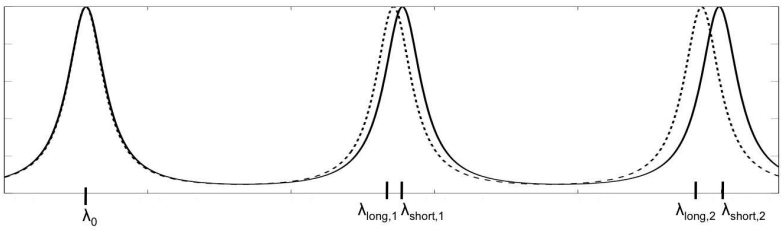

Fig. 7. Transmission spectra of the two individual ring resonators with different optical roundtrip. The resonator with the short optical roundtrip (solid line) has a larger free spectral range than the resonator with the long optical roundtrip (dashed line).

At the wavelength λ_0 two resonances of the respective resonators coincide. Neglecting dispersion, the other resonance wavelengths of both resonators are

$$\lambda_{short,k} = \lambda_0 + k \cdot fsr_{short} \tag{6}$$

$$\lambda_{long,k} = \lambda_0 + k \cdot fsr_{long} \tag{7}$$

with fsr the free spectral range value of the corresponding resonator and k an integer.
Starting from λ_0, an envelope period will be reached when two resonances coincide again. This occurs for an index $k = K$ for which:

$$\lambda_{short,K} = \lambda_{long,K+1} \tag{8}$$

$$\Leftrightarrow \quad K \cdot fsr_{short} = (K+1)\, fsr_{long} \tag{9}$$

$$\Leftrightarrow \quad K = \frac{fsr_{long}}{fsr_{short} - fsr_{long}} \tag{10}$$

The two resonances will only exactly coincide when K is an integer, but when the free spectral range difference between the two resonators in the cascade is small compared to the full-width at half-maximum of the resonance peaks of the individual resonators this period will also be visible when K is not an integer.
The envelope period is given by

$$period = \lambda_{short,K} - \lambda_0 \tag{11}$$

By substituting Eq. (10) in Eq. (6), the formula for the period becomes:

$$period = \frac{fsr_{long}\, fsr_{short}}{fsr_{short} - fsr_{long}} \tag{12}$$

$$= \frac{fsr_{filter}\, fsr_{sensor}}{\left| fsr_{sensor} - fsr_{filter} \right|} \tag{13}$$

B. Derivation and analysis of the analytical function for the constituent peaks in the transmission spectrum of the two cascaded ring resonators

It can be proven that the resonance peaks in the drop spectrum of a single ring resonator can be described in good approximation by a Lorentzian function:

$$T_{drop}(\lambda) = \frac{t_{max}\frac{fwhm^2}{4}}{\frac{fwhm^2}{4} + (\lambda - \lambda_{res})^2} \tag{14}$$

with t_{max} the transmission at resonance, $fwhm$ the full-width at half-maximum of the resonance peak and λ_{res} the resonance wavelength.
Each peak in the transmission spectrum of the two cascaded resonators with different optical roundtrip can therefore be written as the product of two Lorentzian functions that have a slightly different resonance wavelength. We will call these peaks in the transmission spectrum of the cascade the constituent peaks. The transmission of every constituent peak in the spectrum of the cascade can be written as:

$$T_{constituent}(\lambda) = \frac{t_{max,filter}\frac{fwhm^2_{filter}}{4}}{\frac{fwhm^2_{filter}}{4} + \left(\lambda - \lambda_0 - \frac{\Delta\lambda}{2}\right)^2} \cdot \frac{t_{max,sensor}\frac{fwhm^2_{sensor}}{4}}{\frac{fwhm^2_{sensor}}{4} + \left(\lambda - \lambda_0 + \frac{\Delta\lambda}{2}\right)^2} \tag{15}$$

where t_{max} and $fwhm$ are respectively the transmission at resonance and the full-width at half-maximum of the corresponding individual ring resonator, and where λ_0 and $\Delta\lambda$ are respectively the mean of and the difference between the two resonance wavelengths under consideration from both combs.
If we assume that the resonance peaks of both resonators in the cascade have the same $fwhm$, Eq. (15) can be rewritten as:

$$T_{constituent}(\lambda) = \frac{\sqrt{t_{max,filter}t_{max,sensor}}\frac{fwhm^2}{4}}{\frac{fwhm^2}{4} + \left(\lambda - \lambda_0 - \frac{\Delta\lambda}{2}\right)^2} \cdot \frac{\sqrt{t_{max,filter}t_{max,sensor}}\frac{fwhm^2}{4}}{\frac{fwhm^2}{4} + \left(\lambda - \lambda_0 + \frac{\Delta\lambda}{2}\right)^2} \tag{16}$$

The location of the extreme values of this function can be found by solving following equation to λ:

$$\frac{\partial T_{constituent}(\lambda)}{\partial\lambda} = 0 \tag{17}$$

This results in three extreme values at wavelengths

$$\lambda_0, \lambda_0 + \frac{\sqrt{\Delta\lambda^2 - fwhm^2}}{2}, \lambda_0 - \frac{\sqrt{\Delta\lambda^2 - fwhm^2}}{2} \tag{18}$$

This allows us to evaluate the location and values of the maxima of the constituent peaks. We identify two possibilities:

- If the difference between the resonance wavelengths under consideration is larger than the full-width at half-maximum of the individual resonances, $\Delta\lambda > fwhm$, the three extreme values are all real. The constituent peak will in this case have two maxima at $\lambda_{max} = \lambda_0 \pm \frac{\sqrt{\Delta\lambda^2 - fwhm^2}}{2}$ and a local minimum at λ_0. The transmission at each of the two maxima is

  $$T_{max} = \left(\frac{\sqrt{t_{max,filter}t_{max,sensor}}\,fwhm}{2\Delta\lambda}\right)^2 \tag{19}$$

  which quickly converges to zero for increasing values of $\Delta\lambda$. This situation corresponds to the tails of the envelope, where the transmission is very low.

- If however the difference between the resonance wavelengths under consideration is smaller or equal than the full-width at half-maximum of the individual resonators, $\Delta\lambda <= fwhm$, only one of the extreme values in Eq. (18) is real. This situation corresponds to the constituent peaks in the center of the envelope peak, where the transmission is high. In this case the constituent peak has a maximum at its central wavelength λ_0, and the transmission at this maximum is given by

$$T_{max} = \left(\frac{\sqrt{t_{max,filter} t_{max,sensor}}\, fwhm^2}{fwhm^2 + \Delta\lambda^2} \right)^2 \tag{20}$$

C. Derivation of the analytical function for the envelope peak in the transmission spectrum of the two cascaded ring resonators

When the free spectral range difference between the two resonators in the cascade is small compared to the full-width at half-maximum of the resonance peaks of the individual resonators, a periodic envelope signal is superposed on the constituent transmission peaks in the transmission spectrum of the cascade. In every envelope period, there is an envelope peak that is composed of the highest constituent peaks, for which $\Delta\lambda <= fwhm$. In appendix B it is shown that these highest constituent peaks each have one maximum, and the transmission at this maximum is given by

$$T_{max} = \left(\frac{\sqrt{t_{max,filter} t_{max,sensor}}\, fwhm^2}{fwhm^2 + \Delta\lambda^2} \right)^2 \tag{21}$$

where $\Delta\lambda$ is the difference between the two resonance wavelengths corresponding with the considered constituent peak.
We will first consider the special case displayed in Fig. 8 where there exists a wavelength λ_0 at which a resonance peak of the filter ring resonator (solid line) coincides with a resonance peak of the sensor ring resonator (dashed line). At this wavelength λ_0, it holds that $\Delta\lambda_0 = 0$ and the corresponding constituent peak in the transmission spectrum of the cascade will reach the maximum height of the envelope signal. For the next resonance peak of both resonators the resonance wavelength difference is equal to the difference in free spectral range, $\Delta\lambda_1 = \left| fsr_{sensor} - fsr_{filter} \right|$. As proven in appendix B, the corresponding constituent peak will have a maximum at the mean resonance wavelength $\lambda_1 = \lambda_0 + min\left(fsr_{sensor}, fsr_{filter}\right) + \frac{\left| fsr_{sensor} - fsr_{filter} \right|}{2}$.
This reasoning can be generalized to all constituent peaks of the same envelope peak:

$$\Delta\lambda_k = \left| k \cdot \left(fsr_{sensor} - fsr_{filter} \right) \right| \tag{22}$$

$$\lambda_k = \lambda_0 + k \cdot \left(min\left(fsr_{sensor}, fsr_{filter}\right) + \frac{\left| fsr_{sensor} - fsr_{filter} \right|}{2} \right) \tag{23}$$

where k is an integer.
By substituting Eq. (23) in Eq. (22), we get:

$$\Delta\lambda_k = \frac{\left| fsr_{sensor} - fsr_{filter} \right|}{min\left(fsr_{sensor}, fsr_{filter}\right) + \frac{\left| fsr_{sensor} - fsr_{filter} \right|}{2}} \left| \lambda_k - \lambda_0 \right| \tag{24}$$

The second term in the denominator is typically much smaller than the first, so we can neglect the second term

$$\Delta\lambda_k \approx \frac{\left| fsr_{sensor} - fsr_{filter} \right|}{min\left(fsr_{sensor}, fsr_{filter}\right)} \left| \lambda_k - \lambda_0 \right| \tag{25}$$

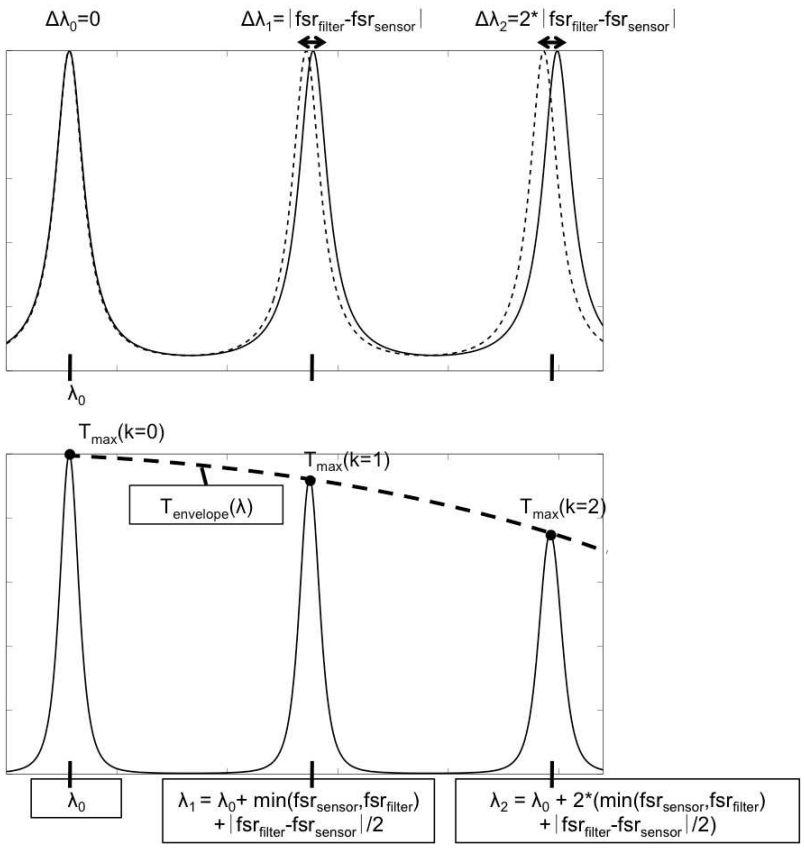

Fig. 8. Top:transmission spectra of the filter ring resonator (solid line) and sensor ring resonator (dashed line). Bottom: transmission spectrum of the cascade of the two ring resonators, showing three different constituent peaks of which the maxima form an envelope signal. This is a special case, where two resonance peaks coincide.

If we substitute Eq. (25) in Eq. (21), we get:

$$T_{max}(k) = \left(\frac{\sqrt{t_{max,filter} t_{max,sensor}} \left(\frac{FWHM}{2}\right)^2}{\left(\frac{FWHM}{2}\right)^2 + (\lambda_k - \lambda_0)^2} \right)^2 \quad (26)$$

$$FWHM = 2 \cdot \frac{fwhm \cdot min\left(fsr_{sensor}, fsr_{filter}\right)}{\left|fsr_{filter} - fsr_{sensor}\right|} \quad (27)$$

This formula gives the peak transmission values of the highest constituent peaks in the central region of the envelope peak, for the special case where there exists a constituent peak that is the product of two coinciding resonance peaks.
It can be generalized to the formula of a continuous function going through the maxima of the constituent peaks, also for the case where there is no perfect coincidence of resonances, by defining $\lambda_{central}$ as the central wavelength of the envelope peak and by substituting λ_0 and λ_k respectively by $\lambda_{central}$ and the continuous wavelength λ:

$$T_{envelope}(\lambda) = \left(\frac{\sqrt{t_{max,filter} t_{max,sensor}} \left(\frac{FWHM}{2}\right)^2}{\left(\frac{FWHM}{2}\right)^2 + (\lambda - \lambda_{central})^2} \right)^2 \quad (28)$$

$$FWHM = 2 \cdot \frac{fwhm \cdot min\left(fsr_{sensor}, fsr_{filter}\right)}{\left|fsr_{filter} - fsr_{sensor}\right|} \tag{29}$$

D. Derivation of the formula for the sensitivity

We consider the special case displayed in Fig. 9 where there exists a wavelength λ_0 at which a resonance peak of the filter ring resonator (solid line) coincides with a resonance peak of the sensor ring resonator (dashed line). At this wavelength λ_0 the corresponding constituent peak in the transmission spectrum of the cascade will reach the maximum height of the envelope signal.

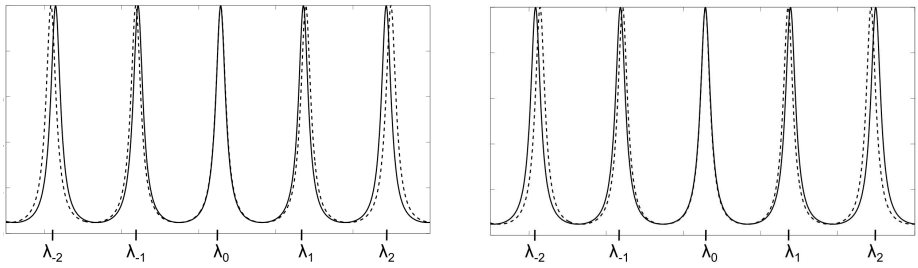

Fig. 9. Transmission spectra of the individual filter ring resonator (solid line) and sensor ring resonator (dashed line) for the case where two resonances of the respective resonators coincide at λ_0. Left: the free spectral range of the filter resonator is larger than the free spectral range of the sensor resonator. Right: the free spectral range of the filter resonator is smaller than the free spectral range of the sensor resonator.

We distinguish two cases:
The first case is illustrated in the left graph in Fig. 9, and occurs when the free spectral range of the filter resonator is larger than the free spectral range of the sensor resonator. When in this case the resonance wavelengths of the sensor ring resonator shift to larger wavelengths over a spectral distance $\left|fsr_{sensor} - fsr_{filter}\right|$, the resonances of the filter and sensor resonators will overlap at wavelength λ_1. The peak of the envelope signal will thus have shifted over a distance fsr_{filter} to larger wavelengths.
The second case is illustrated in the right graph in Fig. 9, and occurs when the free spectral range of the filter resonator is smaller than the free spectral range of the sensor resonator. When in this case the resonance wavelengths of the sensor ring resonator shift to larger wavelengths over a spectral distance $\left|fsr_{sensor} - fsr_{filter}\right|$, the resonances of the filter and sensor resonators will overlap at wavelength λ_{-1}. The peak of the envelope signal will thus have shifted over a distance fsr_{filter} to smaller wavelengths.
From both cases, we can conclude that the sensitivity of the sensor consisting of two cascaded ring resonators is equal to the sensitivity of the sensor ring resonator multiplied by a factor $\frac{fsr_{filter}}{fsr_{filter} - fsrsensor}$. This factor is positive if $fsr_{filter} > fsr_{sensor}$ and negative when $fsr_{filter} < fsr_{sensor}$.
When taking first order dispersion into account, the sensitivity of the sensor ring resonator is

$$\frac{\partial \lambda_{res}}{\partial n_{env}} = \frac{\frac{\partial n_{eff,sensor}}{\partial n_{env}} \lambda}{n_{g,sensor}} \tag{30}$$

with $\frac{\partial \lambda_{res}}{\partial n_{env}}$ the sensitivity defined as the change of the resonance wavelength of the sensor ring resonator due to a change of the environment refractive index, $\frac{\partial n_{eff,sensor}}{\partial n_{env}}$ the change of the

effective index of the sensor ring resonator waveguide due to a change of the refractive index in the environment of the sensor and $n_{g,sensor}$ the group index of the sensor ring resonator waveguide.
The sensitivity of the sensor consisting of two cascaded ring resonators than becomes

$$\frac{\partial \lambda_{central}}{\partial n_{env}} = \frac{\partial \lambda_{central}}{\partial \lambda_{res}} \frac{\partial \lambda_{res}}{\partial n_{env}} \tag{31}$$

$$= \frac{fsr_{filter}}{fsr_{filter} - fsr_{sensor}} \frac{\frac{\partial n_{eff,sensor}}{\partial n_{env}} \lambda}{n_{g,sensor}} \tag{32}$$

with $\frac{\partial \lambda_{central}}{\partial n_{env}}$ the sensitivity defined as the change of the central wavelength of the envelope peak due to a change of the refractive index of the environment of the sensor.

E. Calculation of the theoretical sensitivity of the prototype

To be able to compare the experimentally determined sensitivity of the sensor described in section 4 with the theoretical sensitivity described by Eq. (5), the free spectral range was measured of an individual ring resonator that consisted of a waveguide with the same dimensions as the one of which our sensor consists. From this measurement, the group index of the waveguide was calculated, yielding $n_{g,filter} = 4.217$ when the resonator was covered with silicon oxide and $n_{g,sensor} = 4.404$ when it was immersed in water. Based on these values of the group index we calculated the values of the free spectral range of the filter ring resonator and sensor ring resonator of which our sensor consists to be $fsr_{filter} = 219.6pm$ and $fsr_{sensor} = 211.4pm$ respectively. Using the vectorial mode solver Fimmwave it was calculated for our waveguide that the sensitivity of its effective index to a changing refractive index in an aqueous environment is $\frac{\partial n_{eff,sensor}}{\partial n_{env}} = 0.22$. With these values Eq. (5) yields a theoretical sensitivity of 2085nm/RIU, which corresponds well with the measured value of 2169nm/RIU.
The sensitivity of a single ring resonator can be calculated with

$$\frac{\partial \lambda_{resonance}}{\partial n_{env}} = \frac{\frac{\partial n_{eff,sensor}}{\partial n_{env}} \lambda}{n_{g,sensor}} \tag{33}$$

This results in a sensitivity of 76nm/RIU at a wavelength of 1530nm/RIU.

Acknowledgements

The authors thank *ePIXfab* (`www.epixfab.eu`) for the fabrication of the device, Steven Verstuyft for help during the final steps of the fabrication and Liesbet Van Landschoot for taking the SEM-picture. Tom Claes was supported by the Flemish Institute for the Promotion of Innovation through Science and Technology (IWT) with a specialization grant. This work was performed in the context of the European project InTopSens and the Belgian IAP project Photonics@BE.